ACS SENSORS

pubs.acs.org/acssensors

Article

CuO Nanozymes as Multifunctional Signal Labels for Efficiently Quenching the Photocurrent of ZnO/Au/$AgSbS_2$ Hybrids and Initiating a Strong Fluorescent Signal in a Dual-Mode Microfluidic Sensing Platform

Tingting Wu,[§] Siqi Yu,[§] Li Dai, Jinhui Feng, Xiang Ren, Hongmin Ma, Xueying Wang, Qin Wei,* and Huangxian Ju*

Cite This: *ACS Sens.* 2022, 7, 1732−1739

Read Online

ACCESS | Metrics & More | Article Recommendations | Supporting Information

ABSTRACT: A novel dual-mode microfluidic sensing platform based on CuO nanozymes as a photoelectrochemical (PEC)-fluorescent (FL) multifunctional signal label was developed for ultrasensitive neuron specific enolase (NSE) detection. Herein, ZnO/Au/$AgSbS_2$ hybrids, possessing excellent PEC properties, were first exploited as a sensing matrix to provide a stable photocurrent. The controlled synthesis of photoactive ZnO nanoflowers (NFs) was successfully conducted using a microfluidic reactor in the scale of seconds. Furthermore, the photocurrent of ZnO NFs decorated by Au and $AgSbS_2$ nanoparticles significantly improved, owing to the local surface plasma resonance effect of Au and matching band structure between ZnO and $AgSbS_2$. A strategy of catalytic oxidation ascorbic acid (AA) by CuO nanozymes was proposed to quench the PEC signals and initiate FL signals. CuO nanoparticles growing on conductive carbon spheres (CuO@CSs) as secondary antibodies' labels could efficiently catalyze the oxidation of AA to achieve a PEC "signal-off" state. Then, the produced dehydroascorbic acid reacting with *o*-phenylenediamine opportunely generated a strong FL signal. Importantly, wide linear ranges of 0.0001−150 ng/mL for the PEC technique and 0.001−150 ng/mL for the FL method with a low detection limit of 0.028 and 0.25 pg/mL, respectively, could guarantee the sensitive detection of NSE.

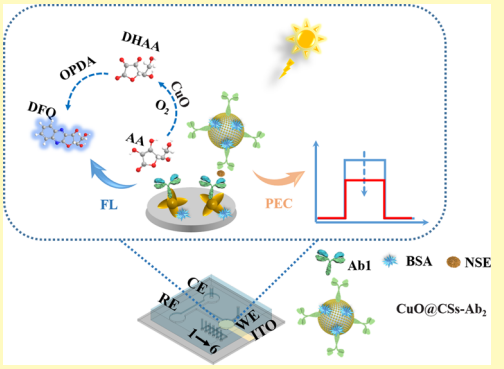

KEYWORDS: *dual-mode, microfluidic sensor, ZnO/Au/$AgSbS_2$, CuO nanozyme, NSE*

Downloaded via NANJING UNIV on June 28, 2022 at 03:41:00 (UTC).
See https://pubs.acs.org/sharingguidelines for options on how to legitimately share published articles.

Photoelectrochemical (PEC) analysis, a newly developing analytical technique, which can convert light energy into readable electrical signal, has attracted great interest.[1,2] Until now, PEC sensors have exhibited a low background signal, high sensitivity, and easy availability in the fields of bioanalysis and environmental molecules detection.[3,4] Nevertheless, the poor anti-interference capability of the PEC methods which depended on as single signal change usually influenced the analytical accuracy.[5] In addition, it is still urgent to realize the miniaturization and automation of the PEC sensor. To solve the defects mentioned above, a rapid and sensitive dual-mode sensing platform integrating PEC with fluorescent (FL) methods based on a microfluidic chip was developed in this work for quantitative analysis of neuron specific enolase (NSE). On the one hand, the distinct dual-response signals are in a position to efficaciously authenticate each other to obviously improve the accuracy of analysis.[6] On the other hand, the designed dual-mode microfluidic biosensor successfully obtained the superiorities of microfluidic devices, such as high portability, low consumption of reagents, and massive parallelization.[7,8]

Efficient signal amplification strategies played a hard-core role in ameliorating the sensitivity of PEC sensors.[9] Among a variety of signal amplification methods, enzyme-mediated reactions such as biocatalytic precipitation and electron donor production which could induce significant changes of signals have attracted great attention.[10,11] However, natural enzymes including alkaline phosphate, peroxidase, and glucose oxidase suffered from the intrinsic defects of high cost, liable to denaturation, and inactivation. It is worth noting that cupric oxide nanoparticles (CuO NPs), as an ascorbate oxidase mimetic, have ignited intensive interest benefiting from their outstanding enzyme-like activity.[12,13] Concretely, CuO NPs could efficiently catalyze the oxidation of ascorbic acid (AA) to

Received: March 7, 2022
Accepted: May 17, 2022
Published: May 26, 2022

ACS Publications

© 2022 American Chemical Society

produce dehydroascorbic acid (DHAA) utilizing O_2 as the oxidant.[14] Inspired by this principle, a novel strategy of consuming AA by CuO nanozymes was proposed to mediate the photoelectric response for achieving the ultrasensitive detection of NSE in this paper. Meanwhile, 3-(1,2-dihydroxyethyl) furo[3,4-*b*]quinoxaline-1-one (DFQ) with a strong FL signal was generated via utilizing DHAA produced by CuO NPs-catalyzed oxidation of AA to react with *o*-phenylenediamine (OPDA), which could serve as a reliable reference for PEC analysis.

More importantly, the exploration of photochemically active materials with high photoelectric conversion efficiency was another kernel process for fabricating high-performance PEC sensors.[15] First, as a kind of semiconductor, zinc oxide (ZnO) was regarded as an outstanding photoelectric material because of the lower recombination rate of photocarriers and good chemical stability.[16,17] Simultaneously, the shape-controlled synthesis is a pivotal task for ZnO because the morphology and structure had decisive influence on its PEC performance.[18] However, traditional methods for ZnO synthesis including the solvothermal method, chemical vapor deposition, and coprecipitation faced great challenges such as the poor control of batch reaction processes and time consumption (at least several hours).[19,20] Microfluidic reactors, possessing high reproducibility and strong automation, provided a new horizon for controllable synthesis of functional nanostructures.[21] Moreover, the designed microfluidic systems are able to intensify the mass and heat transfers and reduce the reaction volume and time because of their narrow channels and variable length.[19,22] Thus, a novel method using microfluidic reactors to precisely control the nucleation and growth of photoactive ZnO nanoflowers (NFs) in a short time was proposed for providing a stable photocurrent in the PEC system. Second, silver antimony sulfide ($AgSbS_2$) with a suitable band gap (1.72 eV) and Au nanoparticles as a sensitizer were first used to greatly heighten the visible-light utilization efficiency of ZnO NFs. On the one hand, $AgSbS_2$ displayed great potential as a marvelous solar absorber benefiting from the high absorption coefficient ($\alpha \sim 10^5$ cm^{-1}).[18] More importantly, the heterojunctions formed between ZnO and $AgSbS_2$ significantly promoted the charge separation of the photoelectric system. On the other hand, the prominent electron conductivity and localized surface plasmon resonance effect of Au nanoparticles could further enhance the photoelectric conversion efficiency of ZnO.

In the present study, an innovative PEC-FL dual-signal microfluidic biosensor based on CuO nanozymes as a multifunctional signal label and ZnO/Au/$AgSbS_2$ composites as a photoactive matrix was first proposed for accurate determination of NSE. NSE, used as a model analyte, is a reliable biomarker for small cell lung cancer. First, the photocurrent of the sensing matrix was significantly improved after ZnO NFs were decorated with Au and the $AgSbS_2$ sensitizer. Second, for realizing ultrasensitive NSE detection, CuO nanozymes possessed remarkable ascorbate oxidase mimetic activity as a multifunctional signal label was utilized to effectively quench the output photocurrent and generate a strong FL signal. As shown in Scheme 1, CSs with a large surface area and high conductivity were introduced to load CuO NPs, and the obtained CuO@CSs were covalently conjugated with Ab_2. Then, with the increasing concentrations of NSE, more CuO@CSs-Ab_2 were incubated on the modified electrode, and the photocurrent decreased while the FL signal

Scheme 1. (A) Synthesis Route of ZnO/Au/$AgSbS_2$, (B) Manufacturing Process of the Dual-Mode Microfluidic Analytical Platforms, and (C) Preparation Procedure of the CuO@CSs-Ab_2 Bioconjugate

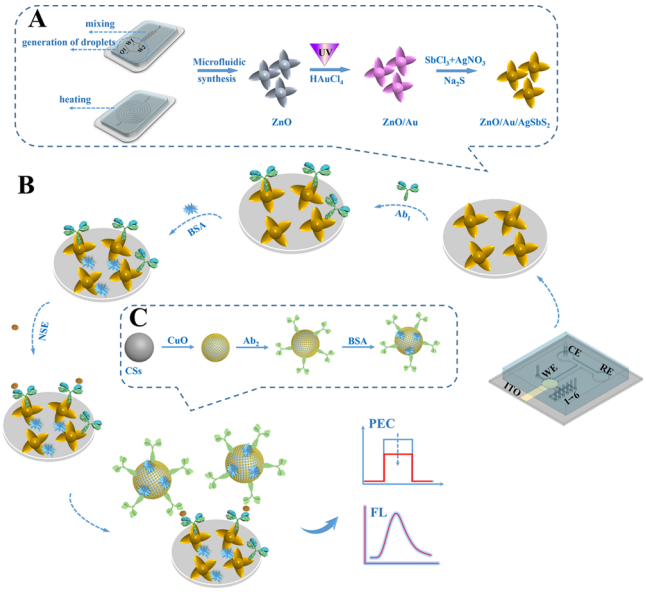

obviously enhanced. More importantly, the catalytic effect of CuO NPs on the microfluidic platform was more obvious than the traditional detection system because of the small reaction volume of the microfluidic platform (Figure S1). Based on the above strategies, the proposed dual-signal microfluidic sensing platform showed ultrahigh sensitivity, specificity, and stability for NSE determination.

EXPERIMENTAL SECTION

Synthesis of Photoactive ZnO NFs. The photoactive ZnO NFs were synthesized through a microfluidic system. As shown in Scheme 1A, the microchannel contains three kinds of zones, the first zone was used for the generation of droplets, and the second zone was for mixing of the precursor solution. Meanwhile, the third was the heating zone with a temperature of 100 °C. The W1 is the inlet of 10 mmol $Zn(CH_3COO)_2$, W2 is the inlet of 30 mmol NaOH, and Q1 is the inlet of mineral oil. The three inlet flows were pumped into the microchannel. The flow rate of W1 and W2 is 2 mL/h while for Q1 is 3 mL/h and the obtained droplet was observed under a microscope with a high-speed camera (Figure S2). The obtained ZnO was collected from the outlet and washed with ethanol four times.

Preparation of Microelectrodes. First of all, ITO slices (6 × 5 cm^2) were cleaned with detergent, acetone, ethanol, and deionized water, severally, and blow-dried with nitrogen. Then, the working microelectrode (WE) was prepared according to previous work (Supporting Information).[7] After that, 15 μL of ZnO NF suspension (4 mg/mL) was modified on the WE. After drying under an infrared lamp, the modified microelectrodes were treated with oxygen plasma treatment for 50 s and then stuck with polydimethylsiloxane microchannels which were obtained using the soft lithographic technique (Supporting Information).

Synthesis of ZnO/Au/$AgSbS_2$ Composites. ZnO/Au was obtained via irradiation with ultraviolet light (main 365 nm, 2000 mW/cm^2). As shown in Scheme 1A, 1% $HAuCl_4$ ethanol/water solution ($V_{ethanol}$:V_{water} = 1:1) was injected into the ZnO WE from inlet 4. Au ions could be reduced by the photogenerated electron produced in ZnO; meanwhile, the ethanol molecule was used as a hole-scavenger.[23] The obtained ZnO/Au was washed with ultrapure water and dried.

https://doi.org/10.1021/acssensors.2c00486
ACS Sens. 2022, 7, 1732−1739

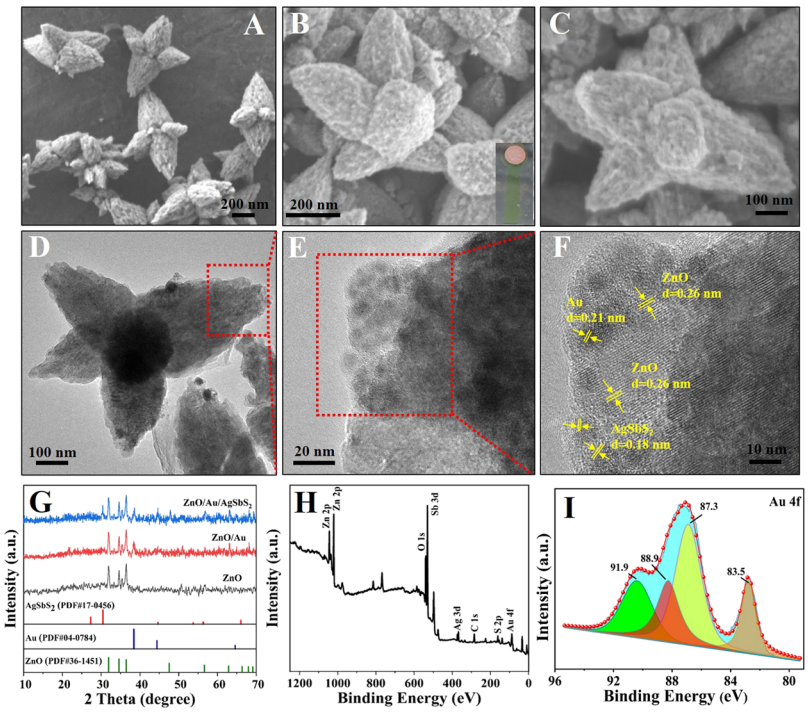

Figure 1. Scanning electron microscopy (SEM) image of (A) ZnO, (B) ZnO/Au, and (C) ZnO/Au/$AgSbS_2$; transmission electron microscopy (TEM) (D) and high-resolution transmission electron microscopy (HRTEM) (E and F) images of ZnO/Au/$AgSbS_2$; (G) X-ray diffraction (XRD) spectrum of ZnO, ZnO/Au, and ZnO/Au/$AgSbS_2$; (H) X-ray photoelectron spectroscopy (XPS) pattern of ZnO/Au/$AgSbS_2$; (I) XPS high-resolution spectrum of Au 4f.

To realize the in situ growth of $AgSbS_2$, 100 μL of $AgNO_3$ ethanol solution (0.1 mol/L) was injected into the ZnO/Au WE from inlet 4 for 1 min and rinsed with ethanol. Then, 100 μL of 0.1 mol/L $SbCl_3$ was injected for 1 min. Finally, 100 μL of 0.1 mol/L Na_2S methanol solution was injected from inlet 4 for 4 min and rinsed with methanol. After repeating three times, ZnO/Au/$AgSbS_2$ was obtained by calcining at 150 °C in N_2 for 1 h.

Preparation of the CuO@CSs-Ab_2 Bioconjugate. First, carbon spheres were obtained according to previous work.[24] The other details can be found in the Supporting Information. Second, CuO@CS composites were prepared as a multifunctional signal label via a facile wet chemical approach.[14] Briefly, 0.15 g of CSs was dispersed in 150 mL of deionized water by ultrasonic treatment for 2 h. After that, 0.59 g of $Cu(CH_3COO)_2$ and 500 μL of glacial acetic acid were added. Then, the mixture was heated to boiling and 10 mL of 40 mg/mL NaOH aqueous solution was added rapidly. After cooling down, the obtained CuO@CSs were washed with ethanol.

For obtaining the CuO@CSs-Ab_2 bioconjugate, 2 mg of CuO@CSs was dispersed in 1 mL of 3 mM thioglycolic acid (TGA) solution containing 100 mM NaCl and shaken for 6 h at 4 °C to introduce the carboxyl groups.[25] Then, 200 μL of EDC/NHS was added and the solution was shaken for 6 h. Subsequently, 1 mL of 10 μg/mL Ab_2 was added under incubation for 10 h. Ultimately, unbound Ab_2 was separated by continuous centrifugation, and the product was dispersed in 1 mL of phosphate-buffered saline (PBS) containing 1% BSA (Scheme 1C).

Manufacturing Process of the Dual-Mode Microfluidic Sensing Platform. As shown in Scheme 1B, for the immobilization of −COOH groups, 15 μL of 3 mmol/L TGA solution was first injected to the ZnO/Au/$AgSbS_2$ WE from inlet 1. After that, 8 μL of EDC/NHS was injected for 30 min to activate the −COOH groups. Then, 15 μL of Ab_1 was injected to WE from inlet 2 and incubated for 1 h. Next, BSA as blocking solution was injected (8 μL, inlet 3), holding for half an hour to shield nonspecific sites. After that, 15 μL of various concentrations of NSE and 15 μL of CuO@CSs-Ab_2 were injected from inlet 5 and inlet 6 and incubated for 1 h, respectively. After each step, the PBS (pH = 7.4) was injected for washing the modified electrode.

PEC and FL Measurements. After the sensing platform was constructed completely, 200 μL of PBS (pH 7.4, 0.1 mol/L) containing 0.1 mol/L AA and OPDA was injected from inlet1 and incubated for 40 min. PEC measurement was performed on a CHI760E electrochemical workstation with a LED lamp (100 W) as the irradiation source. The actual object diagram of the microfluidic analytical platform is shown in Figure S3. After the PEC measurement, the PBS was obtained from the outlet. Fluorescence measurement was conducted on a photoluminescence detection system (excitation wavelength was 350 nm).

RESULTS AND DISCUSSION

Characterization of ZnO/Au/$AgSbS_2$. ZnO/Au/$AgSbS_2$ composites were successfully synthesized and employed as a photoactive matrix to fabricate the dual-mode biosensor. SEM images were applied for exploring morphological characters of the prepared ZnO/Au/$AgSbS_2$ composites. From Figure 1A, the ZnO exhibited a flower-like morphology with a mean diameter around 600 to 800 nm. After the decoration of Au (Figure 1B) and $AgSbS_2$ (Figure 1C) nanoparticles, the surface of ZnO became rougher. Furthermore, the UV−vis absorbance spectra in Figure S4 showed that the characteristic absorption peak of Au (525 nm) was observed, demonstrating the successful preparation of ZnO/Au. The TEM image in Figure 1D demonstrated that ZnO maintained its shape well after the decoration of Au and $AgSbS_2$ nanoparticles. Furthermore, from Figure 1E,F, an interplanar distance of 0.26 nm could be assigned to wurtzite ZnO (JCPDS 36-1451), while an interplanar distance of 0.21 and 0.18 nm was in accordance with the (1 1 1) facet of Au and (2 0 0) facet of $AgSbS_2$, respectively. The above results further displayed that Au and $AgSbS_2$ nanoparticles were tightly distributed on ZnO NFs.

https://doi.org/10.1021/acssensors.2c00486
ACS Sens. 2022, 7, 1732−1739

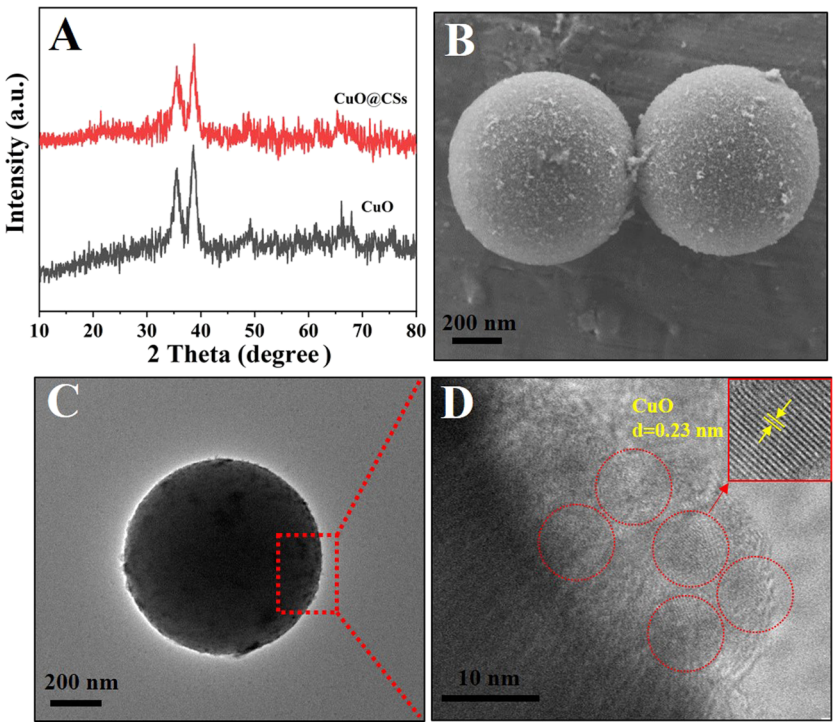

Figure 2. (A) XRD spectrum of CuO and CuO@CSs; SEM (B) and TEM images (C) of CuO@CSs; (D) HRTEM image of CuO@CSs.

Meanwhile, the elemental mapping image of the ZnO/Au/$AgSbS_2$ further displayed a uniform distribution of Au, Ag, Sb, and S elements on ZnO NFs (Figure S5C−H).

Moreover, the XRD analysis was utilized for determining the crystallinity structure of materials. From Figure 1G, the diffraction peaks of ZnO NFs at 31.7°, 34.6°, and 36.2° could be ascribed to the (1 0 0), (0 0 2), and (1 0 1) planes (JCPDS 36-1451). For ZnO/Au, the characteristic peak at 38.4° was attributed to the (1 1 1) plane of Au (JCPDS 04-0784), which indicated that Au nanoparticles exist in the synthesized material. After $AgSbS_2$ decoration, the diffraction peaks of 27.3° and 45.35° corresponding to (1 1 1) and (2 0 0) planes (JCPDS 17-0456) appeared suggesting that ZnO/Au/$AgSbS_2$ composites were successfully prepared.

XPS further analyzed the surface chemical states of ZnO/Au/$AgSbS_2$ hybrids. As presented in Figure 1H, the Zn, O, Au, Ag, Sb, and S elements existing in the survey spectrum were consistent with the EDS spectrum (Figure S5B). Moreover, the XPS spectrum of Au 4f in Figure 1I was fitted into four peaks. The binding energy at 83.5 and 87.3 eV corresponded to Au $4f_{7/2}$ and Au $4f_{5/2}$. Significantly, a negative shift appeared compared with bulk Au (83.8 eV) indicating the strong electronic interaction between the Au and ZnO.[26] The results of XPS analysis in the Supporting Information further proved the successful formation of ZnO/Au/$AgSbS_2$ composites.

Characterization of CuO@CSs. CuO NPs were tightly grown on the surface of CSs and employed as multifunctional signal labels. The XRD patterns in Figure 2A showed the crystallization of CuO@CSs. The distinct diffraction peaks at 35.2° and 38.4° correspond to (0 0 2) and (1 1 1) phases of CuO with a monoclinic structure (JCPDS 72-0629).[14] For CuO@CSs (Figure 2A), a broad peak centered at 22° can be assigned to the CSs which proved that CuO NPs have been successfully anchored on CSs.[24] The SEM images of CuO@CSs further showed that CuO NPs were uniformly distributed on the surface of CSs with a diameter around 750 nm. More significantly, the TEM and HRTEM images are shown in Figure 2C,D, and an interplanar spacing of 0.23 nm was in good agreement with the (1 1 1) crystalline plane of CuO.

Characterization of the Microfluidic Sensing Platform. EIS was provided to probe into the interfacial properties during the fabrication process of the dual-mode sensing platform (Figure 3A). The illustration was Randles equivalent circuit simulated by ZSimWin software (the simulated EIS data are shown in Table S1). In particular, the equivalent circuit contained R_s (solution resistance), R_{et} (electron-transfer

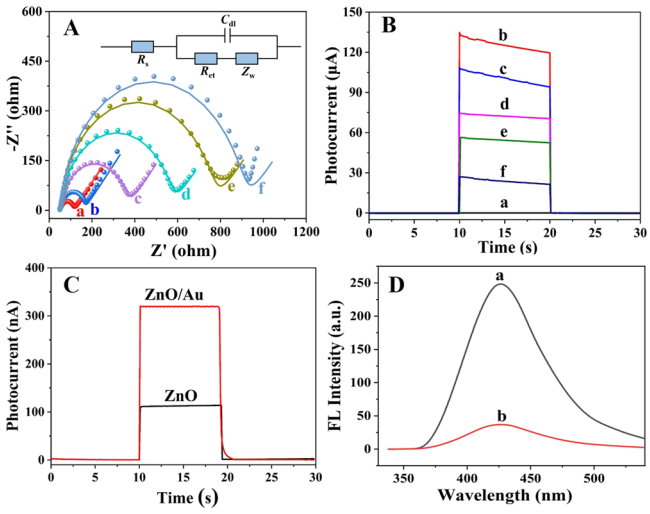

Figure 3. (A) Electrochemical impedance spectroscopy (EIS) Nyquist plots and (B) PEC response of modified electrodes; (C) photocurrent response of ZnO and ZnO/Au;(D) FL intensity of electrolyte solution containing 0.1 mol/L AA and 0.1 mol/L OPDA in the absence and presence of CuO@CSs. The illustrations in A: Randles equivalent circuit for EIS.

https://doi.org/10.1021/acssensors.2c00486
ACS Sens. 2022, 7, 1732−1739

resistance), C_{dl} (double-layer capacitance), and Z_w (Warburg impedance). Among them, R_{et} was equivalent to the semicircle diameter in EIS Nyquist plots, which could represent the interface characteristics of the modified electrodes.[27,28] For bare WE (curve a), a small R_{et} value was exhibited. After the modification of ZnO/Au/$AgSbS_2$ (curve b), Ab_1 (curve c), BSA (curve d), NSE (curve e), and CuO@CSs-Ab_2 (curve f), R_{et} increased gradually, which demonstrated the successful fabrication of the dual-mode biosensor.

The photocurrent signal of each construction step was also investigated in Figure 3B to characterize the fabricated procedure of the dual-mode biosensor. After the decoration of ZnO/Au/$AgSbS_2$, the photocurrent reached maximum (curve b). From Figure 3B, ZnO/Au exhibited a higher photocurrent compared with ZnO. This could be attributed to two reasons as follows: Au nanoparticles with excellent conductivity could accelerate the electron transfer. In addition, Au nanoparticles could absorb the incident light and generate hot electrons.[29] Along with the incubation of Ab_1 (curve c), BSA (curve d), NSE (curve e), and CuO@CSs-Ab_2 (curve f), the photocurrent signal declined step by step indicating that the biosensor is constructed successfully.

The comparison experiments were carried out for verifying the ascorbate oxidase-like activity of CuO@CSs. Figure 3C showed the FL intensity of PBS solution containing 0.1 mol/L AA and 0.1 mol/L OPDA in the absence and presence of CuO@CSs. No obvious FL could be observed in the absence of CuO@CSs (curve a). However, when CuO@CSs were added, a strong FL signal was recorded which indicated that CuO nanoenzymes were equipped to efficiently catalyze the oxidation of AA (curve b).

Possible Mechanism of the Dual-Mode Microfluidic Sensing Platform. Primarily, the UV−vis diffuse-reflectance spectra were utilized to characterize the light absorption performance of ZnO and $AgSbS_2$. From Figure S7A and B, the absorption edges of ZnO and $AgSbS_2$ were located at 387 and 720 nm, respectively. The Tauc plots in the illustration displayed that the bandgap energy (E_g) of ZnO and $AgSbS_2$ was estimated at 3.2 and 1.72 eV.

Moreover, Mott−Schottky analyses of ZnO and $AgSbS_2$ were also performed to determine the electronic band structures. The positive slope in Figure S7C and D indicates n-type semiconductor characteristics for both ZnO and $AgSbS_2$.[30] The flat-band potential (E_{fb}) of ZnO and $AgSbS_2$ was estimated as −0.45 V vs SCE and −0.79 V vs SCE, respectively. For n-type semiconductors, E_{fb} was 0.1 V more positive than conduction band potentials (E_{CB}).[31,32] Thereby, the E_{CB} of ZnO and $AgSbS_2$ was −0.31 V vs NHE and −0.65 V vs NHE. The valence band potential (E_{VB}) of the ZnO was +0.89 V vs NHE and for $AgSbS_2$ it was +1.07 V vs NHE, which can be estimated from the following formula:

$$E_g = E_{VB} - E_{CB}$$

Based on the above analysis, the possible mechanisms of the designed dual-mode biosensor are displayed in Scheme 2. Under visible-light excitation, as the photoactive matrix, ZnO and $AgSbS_2$ were excited to produce photoinduced carriers. Because of the matched band structure, photogenerated electrons were transferred from the CB of $AgSbS_2$ to ZnO and subsequently injected into the ITO, while the holes were driven from the VB of ZnO to $AgSbS_2$ and captured by AA. In addition, benefiting from the excellent electron conductivity and localized surface plasmon resonance effect, Au nanoparticles could further improve the photocurrent.[33] Furthermore, CuO@CSs-Ab_2 were used for photocurrent suppression and inducing a strong fluorescence emission. An obvious decrease of the PEC signal occurred when the CuO@CSs-Ab_2 was immobilized. CuO NPs could act as nanozymes to consume an electron donor as follows: first, with the dissolved O_2 as a green oxidant, CuO exhibited excellent ascorbate oxidase-like activity (eq 1). The oxidation of AA can be further monitored by recording the UV/vis absorbance spectra. As can be seen from Figure S8, AA showed an absorption at 265 nm (curve a); when CuO@CSs were added, the absorbance at 265 nm has declined significantly. Second, as an efficient p-type quencher, CuO could compete with ZnO/Au/$AgSbS_2$ composites for the consumption of light and a hole-trapping agent. Meanwhile, the DHAA obtained from oxidation of AA could react with OPDA to produce FL DFQ (eq 2).

Scheme 2. Possible Mechanism of the Proposed Dual-Mode Biosensor

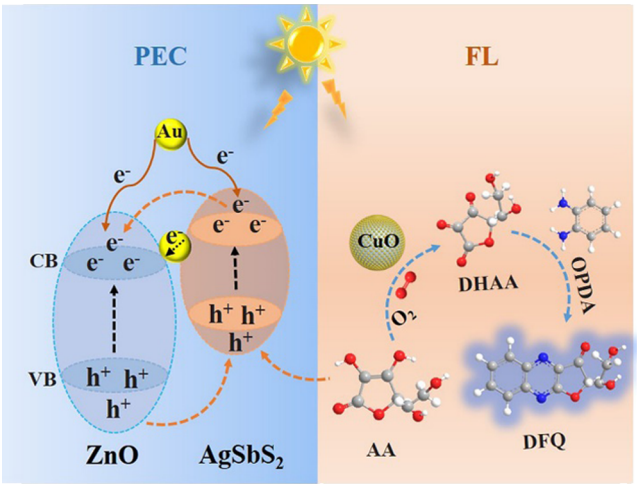

$$AA + O_2 \xrightarrow{CuONPs} DHAA \quad (1)$$

$$DHAA + OPDA \rightarrow DFQ \quad (2)$$

PEC and FL Detection of NSE by the Designed Dual-Mode Microfluidic Sensing Platform. Integrating a PEC method with the FL technique, an innovative microfluidic with dual readout was manufactured for NSE detection. Under optimal conditions (Supporting Information), the PEC and fluorescence responses to NSE were examined. As shown in Figure 4A, the photocurrent response was directly related to the NSE concentration (0.0001−150 ng/mL). With the increment of NSE concentrations, the amount of CuO@CSs-Ab_2 specifically binding to NSE increased, which led to a remarkable decrease in the photocurrent signal. Moreover, the EIS plots of electrodes after incubating with different concentrations of NSE were also explored. As shown in Figure S10 and the simulated data of circuitry elements in Table S2, the EIS responses enhanced gradually with the increasing concentration of NSE from 0.0001 to 150 ng/mL, which indicated that NSE has been successfully captured by Ab_1. Figure 4B showed that the photocurrent response and the logarithm of NSE with different concentrations coincidence with the linear relation. The linear regression equation was I (μA) = − 8.64505 lg c + 20.68547. In addition, the square of the correlation coefficient (R^2) was 0.991 and the detection limit was 0.028 pg/mL (S/N = 3). Moreover, in the presence

https://doi.org/10.1021/acssensors.2c00486
ACS Sens. 2022, 7, 1732−1739

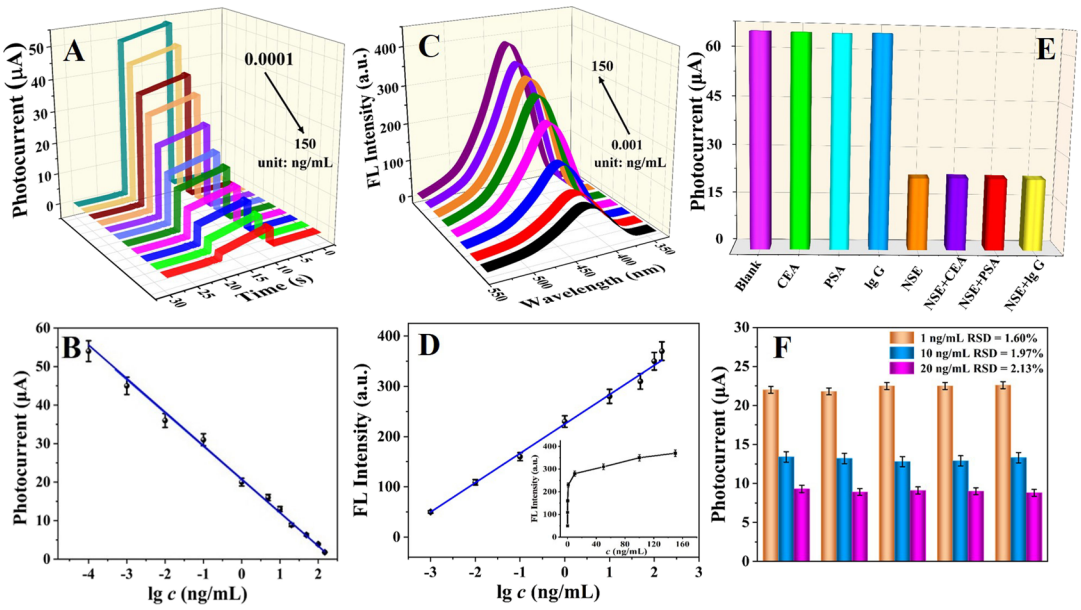

Figure 4. Photocurrent responses (A) and its corresponding calibration curve (B) for detection of NSE (0.0001−150 ng/mL); FL signals (C) and its corresponding calibration curve (D) for the detection of NSE (0.001−150 ng/mL); (E) selectivity test of the microfluidic analytical platforms with CEA, PSA, and IgG as interfering substances. (F) Reproducibility tests of the microfluidic analytical platforms with NSE concentrations of 1, 10, and 20 ng/mL.

of OPDA, NSE could be indirectly detected by measuring the FL intensity. As shown in Figure 4C, the FL intensity enhanced gradually with the increment of NSE (0.001−150 ng/mL). The linear regression equation in Figure 4D could be shown as F = 58.4196 lg c + 225.0431 (R^2 = 0.997), with a detection limit of 0.25 pg/mL (S/N = 3). Compared to other detection methods, the designed dual-mode microfluidic biosensor for detection of NSE possessed outstanding superiorities of a linear range and detection limit (Table S3).

Furthermore, selectivity, reproducibility, and stability were essential for appraising the performance of the designed microfluidic sensing platform.[27] First, to test the selectivity of the fabricated microfluidic biosensor, CEA, PSA, and lg G were used as interfering substances. As depicted in Figure 4E, in the absence of NSE, when interfering substances modified the electrode, no obvious interferential photocurrent signal occurred compared with the blank electrode. In addition, there was no significant change in the photocurrent after 100 ng/mL CEA, PSA, and lg G were mixed respectively with 1 ng/mL NSE, indicating a good selectivity of the as-fabricated microfluidic biosensor. Second, as shown in Figure 4F, five electrodes were prepared separately for detection of different concentration of NSE (1, 10 and 20 ng/mL) under the same conditions. The relative standard deviation (RSD) values of 1.60, 1.97, and 2.13% revealed the satisfactory reproducibility. Third, Figure S10 shows the stability of the microfluidic immunosensor. After the photocurrent was measured at eight on/off irradiation cycles, the photocurrent remains stable indicating that satisfactory stability was obtained. Moreover, the storage stability of the developed microfluidic PEC sensor was also evaluated (Figure S12). After 8 days of storage at 4 °C, the photocurrent intensity of the immunosensor was maintained at 97.3% of the initial photocurrent, showing a good storage stability.

Application of the Developed Dual-Mode Microfluidic Biosensor in Human Serum. The standard addition method was used for evaluating the potential feasibility of the proposed microfluidic biosensor in clinical applications. The human serum samples separated from three normal people were provided by the hospital of the University of Jinan. First, the serum samples were centrifuged at 2800 rpm for 5 min at 4 °C to obtain the supernatants. Then, the human serum samples were diluted with pH 7.4 PBS buffer until the levels were within the calibration range. Finally, standard NSE samples with different concentrations (0.1, 10, and 50 ng/mL) were added to the above diluted human serum samples. As shown in Table 1, the obtained RSD was less than 5% and the recoveries were from 94.0 to 100.6%. The obtained results demonstrated that the dual-mode microfluidic sensing platform could be trustworthily applied for quantitative determination of NSE in human serum samples.

Table 1. Recoveries of NSE in Human Serum Samples

sample (ng/mL)	added (ng/mL)	found (ng/mL)	recovery (%, n = 5)	RSD (%, n = 5)
0.56	0.100	0.654	94.0	3.68
	5.00	5.59	100.6	1.18
	10.0	10.6	100.4	1.23
1.28	0.100	1.39	110.0	2.38
	5.00	6.30	100.4	1.24
	10.0	11.3	100.2	1.22
4.12	0.100	4.22	100.0	1.72
	5.00	9.12	100.0	1.21
	10.0	14.2	100.8	1.21

CONCLUSIONS

In summary, an innovative dual-mode microfluidic sensing platform based on the remarkable ascorbate oxidase mimetic activity of CuO nanozymes was manufactured which realized both PEC and FL detection of NSE. ZnO/Au/$AgSbS_2$ composites with excellent photoactive were first synthesized in a microfluidic reactor and utilized to provide a high PEC

https://doi.org/10.1021/acssensors.2c00486
ACS Sens. 2022, 7, 1732−1739

signal. To realize the accurate NSE detection, CuO@CSs were incubated with secondary antibodies, which effectively quenched the photocurrent via the catalytic effect of CuO NPs toward AA. In addition, an obvious FL signal was subsequently generated because of the reaction between OPDA and the DHAA. On the basis of the above sensing strategy, the dual-mode biosensor achieved ultrasensitive NSE detection in the range of 0.0001−150 ng/mL for the PEC technique and 0.001−150 ng/mL for the FL method. The low detection limits of 0.028 pg/mL for the PEC method and 0.25 pg/mL the FL method were obtained, along with favorable stability, reproducibility, and selectivity. More importantly, the introduction of a microfluidic device makes it possible to achieve miniaturization and automation of the biosensor. This work puts forward a new idea of utilizing nanozymes not only as a quencher of the PEC signal but also to initiate FL signals which could provide a new strategy for constructing a high-efficiency dual-mode biosensing platform to detect biomarkers in human serum.

■ ASSOCIATED CONTENT

Supporting Information

The Supporting Information is available free of charge at https://pubs.acs.org/doi/10.1021/acssensors.2c00486.

Reagents and instruments, synthesis of graphite oxide, microelectrode preparation, FL intensity emission spectra of DFQ in the microfluidic platform and traditional detection system, the designed and the actual object diagram of the designed microchannel for the synthesis of ZnO and the droplet under a microscope with a high-speed camera, the actual object diagram of the microfluidic analytical platform, UV−Vis absorbance spectra of ZnO, Au, and ZnO/Au, SEM image and elemental mapping of ZnO/Au/$AgSbS_2$, XRD patterns of CuO@CSs, UV−vis DRS and Mott−Schottky curves of ZnO and $AgSbS_2$, UV/Vis absorbance spectra of AA and AA-O_2-CuO@CSs, effects of $AgSbS_2$ SILAR cycles, pH of PBS, AA concentration and the incubation time on the photocurrent response, the Nyquist plots of electrodes incubated with different concentrations of NSE and simulation parameters, the stability of the developed microfluidic sensing platform, simulation parameters of the equivalent circuit components, and a comparison of different methods for the detection of NSE (PDF)

■ AUTHOR INFORMATION

Corresponding Authors

Qin Wei − *Collaborative Innovation Center for Green Chemical Manufacturing and Accurate Detection, Key Laboratory of Interfacial Reaction & Sensing Analysis in Universities of Shandong, University of Jinan, Jinan, Shandong 250022, China;* orcid.org/0000-0002-3034-8046; Email: sdjndxwq@163.com

Huangxian Ju − *Collaborative Innovation Center for Green Chemical Manufacturing and Accurate Detection, Key Laboratory of Interfacial Reaction & Sensing Analysis in Universities of Shandong, University of Jinan, Jinan, Shandong 250022, China; State Key Laboratory of Analytical Chemistry for Life Science, Department of Chemistry, Nanjing University, Nanjing 210023, China;* orcid.org/0000-0002-6741-5302; Email: hxju@nju.edu.cn

Authors

Tingting Wu − *Collaborative Innovation Center for Green Chemical Manufacturing and Accurate Detection, Key Laboratory of Interfacial Reaction & Sensing Analysis in Universities of Shandong, University of Jinan, Jinan, Shandong 250022, China*

Siqi Yu − *State Key Laboratory of Analytical Chemistry for Life Science, Department of Chemistry, Nanjing University, Nanjing 210023, China*

Li Dai − *Collaborative Innovation Center for Green Chemical Manufacturing and Accurate Detection, Key Laboratory of Interfacial Reaction & Sensing Analysis in Universities of Shandong, University of Jinan, Jinan, Shandong 250022, China*

Jinhui Feng − *Collaborative Innovation Center for Green Chemical Manufacturing and Accurate Detection, Key Laboratory of Interfacial Reaction & Sensing Analysis in Universities of Shandong, University of Jinan, Jinan, Shandong 250022, China*

Xiang Ren − *Collaborative Innovation Center for Green Chemical Manufacturing and Accurate Detection, Key Laboratory of Interfacial Reaction & Sensing Analysis in Universities of Shandong, University of Jinan, Jinan, Shandong 250022, China;* orcid.org/0000-0002-4321-4282

Hongmin Ma − *Collaborative Innovation Center for Green Chemical Manufacturing and Accurate Detection, Key Laboratory of Interfacial Reaction & Sensing Analysis in Universities of Shandong, University of Jinan, Jinan, Shandong 250022, China;* orcid.org/0000-0002-7061-8944

Xueying Wang − *Collaborative Innovation Center for Green Chemical Manufacturing and Accurate Detection, Key Laboratory of Interfacial Reaction & Sensing Analysis in Universities of Shandong, University of Jinan, Jinan, Shandong 250022, China*

Complete contact information is available at: https://pubs.acs.org/10.1021/acssensors.2c00486

Author Contributions

[§]T.W. and S.Y. contributed equally to this work.

Notes

The authors declare no competing financial interest.

■ ACKNOWLEDGMENTS

This study was supported by the National Key Scientific Instrument and Equipment Development Project of China (No. 21627809), National Natural Science Foundation of China (No. 21777056), Special Foundation for Taishan Scholar Professorship of Shandong Province, Jinan Scientific Research Leader Workshop Project (2018GXRC024 and 2018GXRC021), and the Innovation Team Project of Colleges and Universities in Jinan (No.2019GXRC027).

■ REFERENCES

(1) Fan, G. C.; Shi, X. M.; Zhang, J. R.; Zhu, J. J. Cathode Photoelectrochemical Immunosensing Platform Integrating Photocathode with Photoanode. *Anal. Chem.* **2016**, *88*, 10352−10356.

(2) Wen, G. M.; Ju, H. X. Enhanced Photoelectrochemical Proximity Assay For Highly Selective Protein Detection in Biological Matrixes. *Anal. Chem.* **2016**, *88*, 8339−8345.
(3) Liu, S. H.; Jia, Y.; Dong, H.; Yu, X. D.; Zhang, D. P.; Ren, X.; Li, Y. Y.; Wei, Q. Intramolecular Photoelectrochemical System Using Tyrosine-Modified Antibody-Targeted Peptide as Electron Donor for Detection of Biomarkers. *Anal. Chem.* **2020**, *92*, 10935−10939.
(4) Yan, T.; Wu, T. T.; Wei, S. Y.; Wang, H. Q.; Sun, M.; Yan, L. G.; Wei, Q.; Ju, H. X. Photoelectrochemical Competitive Immunosensor for 17β-estradiol Detection based on $ZnIn_2S_4$@NH_2-MIL-125(Ti) Amplified by PDA NS/Mn: ZnCdS. *Biosen. Bioelectron.* **2020**, *148*, No. 111739.
(5) Wei, J.; Chang, W.; Qileng, A.; Liu, W.; Zhang, Y.; Rong, S.; Lei, H.; Liu, Y. Dual-modal Split-type Immunosensor for Sensitive Detection of Microcystin-LR: Enzymeinduced Photoelectrochemistry and Colorimetry. *Anal. Chem.* **2018**, *90*, 9606−9613.
(6) Mei, L. P.; Jiang, X. Y.; Yu, X. D.; Zhao, W. W.; Xu, J. J.; Chen, H. Y. Cu Nanoclusters-encapsulated Liposomes: Toward Sensitive Liposomal Photoelectrochemical Immunoassay. *Anal. Chem.* **2018**, *90*, 2749−2755.
(7) Feng, J. H.; Dai, L.; Ren, X.; Ma, H. M.; Wang, X. Y.; Fan, D. W.; Wei, Q.; Wu, R. D. Self-powered Cathodic Photoelectrochemical Aptasensor Comprising a Photocathode and a Photoanode in Microfluidic Analysis Systems. *Anal. Chem.* **2021**, *93*, 7125−7132.
(8) Singh, N.; Ali, M. A.; Rai, P.; Sharma, A.; Malhotra, B.; John, R. Microporous Nanocomposite Enabled Microfluidic Biochip for Cardiac Biomarker Detection. *ACS Appl. Mater. Interfaces* **2017**, *9*, 33576−33588.
(9) Li, F.; Zhou, Y. L.; Yin, H. S.; Ai, S. Y. Recent Advances On Signal Amplification Strategies In Photoelectrochemical Sensing of MicroRNAs. *Biosens. Bioelectron.* **2020**, *166*, No. 112476.
(10) Zhao, W. W.; Ma, Z. Y.; Yu, P. P.; Dong, X. Y.; Xu, J. J.; Chen, H. Y. Highly Sensitive Photoelectrochemical Immunoassay With Enhanced Amplification Using Horseradish Peroxidase Induced Biocatalytic Precipitation On a CdS Quantum Dots Multilayer Electrode. *Anal. Chem.* **2012**, *84*, 917−923.
(11) Zhuang, J.; Han, B.; Liu, W.; Zhou, J.; Liu, K.; Yang, D.; Tang, D. Liposome-amplified Photoelectrochemical Immunoassay for Highly Sensitive Monitoring of Disease Biomarkers based on a Split-type Strategy. *Biosens. Bioelectron.* **2018**, *99*, 230−236.
(12) Chen, W.; Chen, J.; Feng, Y. B.; Hong, L.; Chen, Q. Y.; Wu, L. F.; Lin, X. H.; Xia, X. H. Peroxidase-like Activity of Water-soluble Cupric Oxide Nanoparticles and Its Analytical Application for Detection of Hydrogen Peroxide and Glucose. *Analyst* **2012**, *137*, 1706−1712.
(13) He, S. B.; Balasubramanian, P.; Hu, A. L.; Zheng, X. Q.; Lin, M. T.; Xiao, M. X.; Peng, H. P.; Deng, H. H.; Chen, W. One-pot Cascade Catalysis At Neutral pH Driven By CuO Tandem Nanozyme For Ascorbic Acid and Alkaline Phosphatase Detection. *Sens. Actuators, B* **2020**, *321*, No. 128511.
(14) He, S. B.; Hu, A. L.; Zhuang, Q. Q.; Peng, H. P.; Deng, H. H.; Chen, W.; Hong, G. L. Ascorbate Oxidase Mimetic Activity of Copper (II) Oxide Nanoparticles. *ChemBioChem* **2020**, *21*, 978−984.
(15) Bao, C. Z.; Fan, D. W.; Liu, X.; Wang, X. Y.; Wu, D.; Ma, H. M.; Hu, L. H.; Wang, H.; Sun, X.; Wei, Q. A Signaloff Type Photoelectrochemical Immunosensor for the Ultrasensitive Detection of Procalcitonin: Ru (bpy) $_3^{2+}$ and Bi_2S_3 Co-sensitized $ZnTiO_3$/TiO_2 Polyhedra as Matrix and Dual Inhibition by SiO_2/PDA-Au. *Biosens. Bioelectron.* **2019**, *142*, No. 111513.
(16) Han, F. J.; Song, Z. Q.; Nawaz, M. H.; Dai, M. J.; Han, D. F.; Han, L. P.; Fan, Y. Y.; Xu, J. N.; Han, D. X.; Niu, L. MoS_2/ZnO-Heterostructures-Based Label-Free, Visible-Light-Excited Photoelectrochemical Sensor for Sensitive and Selective Determination of Synthetic Antioxidant Propyl Gallate. *Anal. Chem.* **2019**, *91*, 10657−10662.
(17) Wang, J.; Yang, Z.; Gao, X.; Yao, W.; Wei, W.; Chen, X.; Zong, R.; Zhu, Y. Core-shell g-C_3N_4@ZnO Composites as Photoanodes with Double Synergistic Effects for Enhanced Visible-light Photoelectrocatalytic Activities. *Appl. Catal., B* **2017**, *217*, 169−180.
(18) Han, J. H.; Liu, Z. F.; Guo, K. Y.; Zhang, X.; Hong, T. T.; Wang, B. $AgSbS_2$ Modified ZnO Nanotube Arrays for Photoelectrochemical Water Splitting. *Appl. Catal., B* **2015**, *179*, 61−68.
(19) Hao, N. J.; Xu, Z.; Nie, Y.; Jin, C. R.; Closson, A. B.; Zhang, M.; Zhang, J. X. Microfluidics-Enabled Rational Design of ZnO Micro-/Nanoparticles with Enhanced Photocatalysis, Cytotoxicity, and Piezoelectric Properties. *Chem. Eng. J.* **2019**, *378*, No. 122222.
(20) Moezzi, A.; McDonagh, A. M.; Cortie, M. B. Zinc oxide particles: Synthesis, Properties and Applications. *Chem. Eng. J.* **2012**, *185*, 1−22.
(21) Elvira, K. S.; Wootton, R. C.; deMello, A. J. The Past, Present and Potential for Microfluidic Reactor Technology in Chemical Synthesis. *Nat. Chem.* **2013**, *5*, 905−915.
(22) Paseta, L.; Seoane, B.; Julve, D.; Sebastián, V.; Téllez, C.; Coronas, J. Accelerating the Controlled Synthesis of Metal−Organic Frameworks by a Microfluidic Approach: A Nanoliter Continuous Reactor. *ACS Appl. Mater. Interfaces* **2013**, *5*, 9405−9410.
(23) Xu, L. L.; Zhang, H.; Tian, Y.; Jiao, A. X.; Chen, F.; Chen, M. Photochemical Synthesis of ZnO@ Au Nanorods As an Advanced Reusable SERS Substrate for Ultrasensitive Detection of Light-resistant Organic Pollutant in Wastewater. *Talanta* **2019**, *194*, 680−688.
(24) Tang, S.; Tang, Y.; Vongehr, S.; Zhao, X.; Meng, X. Nanoporous Carbon Spheres and Their Application in Dispersing Silver Nanoparticles. *Appl. Surf. Sci.* **2009**, *255*, 6011−6016.
(25) Jia, Y.; Yang, L.; Xue, J. W.; Zhang, N.; Fan, D. W.; Ma, H. M.; Ren, X.; Hu, L. H.; Wei, Q. Bioactivity-Protected Electrochemiluminescence Biosensor Using Gold Nanoclusters As The Low-potential Luminophor and Cu_2S Snowflake as Co-reaction Accelerator for Procalcitonin Analysis. *ACS Sens.* **2019**, *4*, 1909−1916.
(26) Yang, T. H.; Huang, L. D.; Harn, Y. W.; Lin, C. C.; Chang, J. K.; Wu, C. I.; Wu, J. M. High Density Unaggregated Au Nanoparticles on ZnO Nanorod Arrays Function as Efficient and Recyclable Photocatalysts for Environmental Purification. *Small* **2013**, *9*, 3169−3182.
(27) Liu, S.; Jia, Y.; Li, Y.; Wang, P.; Xu, Z.; Liu, Q.; Li, Y.; Wei, Q. Separation of Biological Events From the Photoanode: Toward the Ferricyanide-mediated Redox Cyclic Photoelectrochemical System of an Integrated Photoanode and Photocathode. *ACS Sens.* **2020**, *5*, 3540−3546.
(28) Feng, J.; Li, N.; Du, Y.; Ren, X.; Wang, X.; Liu, X.; Ma, H.; Wei, Q. Ultrasensitive Double-Channel Microfluidic Biosensor-Based Cathodic Photo-electrochemical Analysis via Signal Amplification of SOD-Au@PANI for Cardiac Troponin I Detection. *Anal. Chem.* **2021**, *93*, 14196−14203.
(29) Ruan, Y. F.; Zhang, N.; Zhu, Y. C.; Zhao, W. W.; Xu, J. J.; Chen, H. Y. Photoelectrochemical Bioanalysis Platform of Gold Nanoparticles Equipped Perovskite Bi_4NbO_8Cl. *Anal. Chem.* **2017**, *89*, 7869−7875.
(30) Wu, T. T.; Yan, T.; Zhang, X.; Feng, Y. X.; Wei, D.; Sun, M.; Du, B.; Wei, Q. A Competitive Photoelectrochemical Immunosensor For the Detection of Diethylstilbestrol Based On an Au/UiO-66 (NH_2)/CdS Matrix and a Direct Z-scheme Melem/CdTe heterojunction as Labels. *Biosens. Bioelectron.* **2018**, *117*, 575−582.
(31) Chen, G. J.; Qin, Y.; Jiao, L.; Huang, J. J.; Wu, Y.; Hu, L. Y.; Gu, W. L.; Xu, D. C.; Zhu, C. Z. Nanozyme-Activated Synergistic Amplification for Ultrasensitive Photoelectrochemical Immunoassay. *Anal. Chem.* **2021**, *93*, 6881−6888.
(32) Yan, T.; Zhang, X.; Ren, X.; Lu, Y. Z.; Li, J. K.; Sun, M.; Yan, L. G.; Wei, Q.; Ju, H. X. Fabrication of N-GQDs and $AgBiS_2$ Dual-sensitized ZIFs-derived Hollow $ZnxCo_{3-x}O_4$ Dodecahedron for Sensitive Photoelectrochemical Aptasensing of Ampicillin. *Sens. Actuators, B* **2020**, *320*, No. 128387.
(33) Qian, Y. R.; Feng, J. H.; Wang, H.; Fan, D. W.; Jiang, N.; Wei, Q.; Ju, H. X. Sandwich-type Signal-off Photoelectrochemical Immunosensor Based On Dual Suppression Effect of PbS Quantum Dots/Co_3O_4 Polyhedron as Signal Amplification for Procalcitonin Detection. *Sens. Actuators, B* **2019**, *300*, No. 127001.

https://doi.org/10.1021/acssensors.2c00486
ACS Sens. 2022, 7, 1732−1739